Influence of the sequential purification of biomass-derived carbon dots on their colloidal and optical properties

Andrea S Gonzalez-Vera, Carlos A Pineda-Arellano, Armando Ramírez-Monroy, J. Matos, Luis F Chazaro-Ruiz, J. Rene Rangel-Mendez, Conchi Maria Concepcion Ovin Ania

Carbon Trends 19 (2025) 100460

Contents lists available at ScienceDirect

Carbon Trends

journal homepage: www.elsevier.com/locate/cartre

Influence of the sequential purification of biomass-derived carbon dots on their colloidal and optical properties

Andrea S. Gonzalez-Vera [a,b], Carlos A. Pineda-Arellano [c], Armando Ramírez-Monroy [d], J. Matos [e], Luis F. Chazaro-Ruiz [a,*], J. Rene Rangel-Mendez [a,*], Conchi O. Ania [b,f,*]

[a] División de Ciencias Ambientales, Instituto Potosino de Investigación Científica y Tecnológica A.C., Camino a la Presa de San José 2055, 78216 San Luis Potosí, México
[b] CEMHTI (CNRS UPR 3079) Université d'Orléans, 45071, Orléans, France
[c] Centro de Investigaciones en Óptica, A.C., Unidad Aguascalientes, Pról. Constitución 607, Fraccionamiento Reserva Loma Bonita, Aguascalientes, 20200, México
[d] Lab. Química Coordinación y Organometálica, Centro de Química del Instituto de Ciencias, Benemérita Universidad Autónoma de Puebla, 72570, Puebla, México
[e] Unidad de Cambio Climático y Medio Ambiente (UCCMA), Instituto Iberoamericano de Desarrollo Sostenible, Universidad Autónoma de Chile, Temuco 4780000, Chile
[f] Centre of Advanced Research in Bionanoconjugates and Biopolymers, "Petru Poni" Institute of Macromolecular Chemistry, Iasi, Romania

ARTICLE INFO

Keywords:
Carbon Dots
Sequential filtration
Photoluminescence

ABSTRACT

The purification of photoluminescent carbon dots has a strong impact on their applications, making rigorous protocols necessary to isolate them. In this work, a sequential filtration process was implemented on photoluminescent carbon dots synthesized by a microwave-assisted hydrothermal treatment of an agricultural waste, achieving good effectiveness and higher yields compared to chromatographic purification approaches. Filtration membranes of different cut-offs were carefully selected considering the by-products from the biomass decomposition. The synthetic route allowed the preparation of carbon dots with average particle sizes of 3.5 nm, composed of a graphitic-like core decorated with oxygen and nitrogen moieties. Dynamic light scattering measurements of the suspensions revealed higher aggregation of the nanoparticles in the least purified samples. This also influences the photoluminescence emission properties due to self-absorbing and quenching effects. The thermal characterization of the solids recovered after each filtration step has shown (for the least purified samples) the presence of fragments assigned to molecules arising from an incomplete hydrothermal transformation of the precursor. The aqueous suspension of the carbon dots recovered after the most purified protocol displayed a notorious emission upon excitation at 375 nm, confirming that the carbon dots are responsible for the observed optical features. These results highlight the importance of an adequate purification process of carbon dots obtained from complex precursors (such as biomass), to avoid bias interpretation of their photoluminescence properties.

1. Introduction

Carbon dots (CDs) are carbon-based nanomaterials of nanometric dimensions and singular electron acceptor and donor capacities and intriguing optical properties [1] that have been implemented as sensitizers in solar cells [2], sensors for detection of heavy metals, organics, and bacteria [3–5], and in many other applications [7]. These nanoparticles have been obtained from different carbon sources and by different synthesis methods, such as bottom-up treatments (e.g. chemical oxidation, thermal decomposition, ultrasonic treatment, and hydrothermal synthesis) and top-down approaches (e.g. electrochemical oxidation, acid refluxing, plasma treatment, and laser ablation) [8–12]. The synthesis of CDs using biomass as precursor is a promising method to obtain these valuable nanomaterials from agro-industrial waste, which is an abundant and low-cost sustainable source. However, when biomass is submitted to hydrothermal processes, most of it remains as a solid carbonized material, and the recovered supernatant contains just a few milligrams of CDs along with by-products capable of being in suspension too. The generation of a considerable number of by-products after the hydrothermal process is corroborated by the low yields of CDs obtained from each synthesis [12,13]. The hydrophilic by-products may interact with the highly functionalized CDS, hindering their purification process. An inadequate purification process may impact the performance of the material in the intended application [14–17].

* Corresponding authors.
E-mail addresses: luis.chazaro@ipicyt.edu.mx (L.F. Chazaro-Ruiz), rene@ipicyt.edu.mx (J.R. Rangel-Mendez), conchi.ania@cnrs-orleans.fr (C.O. Ania).

https://doi.org/10.1016/j.cartre.2025.100460
Received 28 September 2024; Received in revised form 23 December 2024; Accepted 6 January 2025
Available online 7 January 2025

Rigorous purification protocols are necessary to achieve the isolation of CDs. Chromatography [17] and liquid-liquid extraction [15] have been employed to perform the purification, however, these techniques can be time-consuming or methodologically complex due to the similarities in the physicochemical properties of the components of the mixture, and the diversity in size, defects, and surface functional groups of the CDs [8]. These processes can be even more challenging in the case of biomass derived CDs due to the heterogeneity of precursors like banana, mango, potato or orange peel [12,18].

On the contrary, membrane separation processes may be a suitable option to achieve the purification of CDs with higher yields than other techniques, since these are facilitated by the high stability of CDs in aqueous suspensions, enabling their separation through a size exclusion mechanism. Membrane separation processes are also a fast and suitable solution towards scaling up for commercialization purposes [19]. For the ultrafiltration membrane separation process, the retention rating parameter used is called molecular weight cutoff (MWCO), and its units of measurement are Daltons, which are also known as atomic mass units [20]. The MWCO from 1 to 500 kDa of a membrane is associated with its ability to retain particles with a size between 1 and 30 nm in diameter [21]. The selection of the retention rating of the membranes is crucial for the implementation of a purification method [22]. Although in the case of CDs there is no direct correlation between the size of the particles and their molecular weight, it is possible to calculate the last one indirectly by estimating their theoretical molecular structure. Sk *et al.*, performed computational studies on carbon dots nanostructures that associated particle sizes between 0.5 and 5.5 nm with molecular weights between 0.1 and 10.8 kDa [23] by counting the carbon atoms in the molecular models.

In this work, a sequential membrane separation process for the purification of carbon dots is proposed. Despite the number of studies reporting the synthesis and different applications of orange peel-derived carbon dots [1–4,6,24–26], the correlations of their chemical composition and structure with the photoluminescence emission properties have been scarcely addressed. Hence in this study, aqueous suspensions of carbon dots obtained from the microwave-assisted hydrothermal treatment of orange peels, were sequentially filtered through membranes of different pore diameters, in the following order of retention rates: 0.22 μm, 0.1 μm, 100 kDa, 50 kDa, and 5 kDa. The samples from the different purification steps were analyzed to obtain information about the chemical composition of the carbon dots, the average particle size in the aqueous suspensions, and the dependence of those parameters on the photoluminescence emission features. Our data has revealed that the low purification steps render large aggregates of carbon dot particles, while average nanoparticles below 10 nm are stabilized for the most purified samples. The aqueous suspension of the carbon dots recovered after the most purified protocol displayed a notorious emission upon excitation at 375 nm, confirming that the carbon dots are responsible for the observed optical features. The samples with low purification showed higher photoluminescence features, partially arising from the presence of subproducts arising from an incomplete hydrothermal transformation of the precursor. These results highlight the critical role of the purification process of carbon dots prepared from complex precursors (such as biomass).

2. Materials and methods

2.1. Synthesis of the CDs

Oranges (*Citrus sinensis)* were collected from a local market in the city of San Luis Potosi, Mexico. To avoid modifications in the composition, origin of the fruit or maturation stage, only the lignocellulosic fraction of oranges from Citrus sinensis species were considered for this study. The peel was carefully removed from the fruit, cut into small pieces, sun dried, and pulverized. Based on previous studies , the as-obtained orange powders were treated in 1 M HCl solution and stirred for 24 hours before further processing [2], to decrease the large inorganic fraction (ashes) in the pristine biomass (Table S2). Afterwards, the liquid was filtered out and the powder was rinsed with deionized water until constant pH (ca. 4), and then dried. The CDs were synthesized through a microwave-assisted hydrothermal method optimized in a previous study [2]. Briefly, 100 mg of the acid-washed orange peel powders were suspended in 15 mL of deionized water and placed in a microwave oven (Nanowave 400 Anton Paar GmbH, maximum power 700 W) at 220 °C for 30 minutes, under stirring at 1000 rpm. The obtained aqueous suspension was sequentially filtered as indicated below.

2.2. Sequential purification

The aqueous suspension recovered from the microwave digestion of the biomass precursor was sequentially filtrated in various steps using membranes of different cut-offs. Details of the membranes and the sequential order in the filtration are as follows: (step 1) mixed-cellulose esters membrane with a pore size of 0.22 μm; (step 2) PVDF Durapore membrane with a pore size of 0.1 μm; (steps 3 to 5) Spectrum MicroKros TC Hollow Fiber Filters with modified poly(ether-sulfone) membranes with a molecular weight cut-off of 100 kDa (step 3), 50 KDa (step 4) and 5 kDa (step 5). The obtained filtrates were freeze-dried to obtain the final CDs-containing powder. The solids were labeled according to the last membrane used in the sequential filtration (e.g., 1:0.22 μm for step 1; 2:0.1 μm for steps 1+ 2; 3:100 kDa for steps 1+2+3; 4:50 kDa for steps 1+2+3+4 and 5:5 kDa for steps 1+2+3+4+5). As example, the sample 4:50 kDa was obtained after 4 sequential filtration steps with membranes of 0.22 μm, followed by 0.1 μm, 100 kDa and finally 50 KDa. The recovered solids after lyophilization were dispersed in deionized water for further characterization of the aqueous suspensions (photoluminescence and UV–vis spectrophotometry).

2.3. Characterization techniques

Fourier Transformed-Infrared Spectroscopy (FTIR) spectra were obtained with an Thermo Scientific NICOLET iS50 FT-IR spectrometer. For this analysis, the materials were dried and measured at Attenuated total reflectance (ATR) mode. Thermogravimetric analyses of the samples were carried out in a thermobalance (Netzsch-STA 409 CD) coupled to a mass spectrometer. Briefly, ca. 10 mg of the sample was heated under an argon atmosphere up to 1000 °C (heating rate of 10 °C min^{-1}) and the composition of the evolved gases was analyzed in the mass spectrometer. The average hydrodynamic diameter size of the materials was determined by electrophoresis by a NANOTRAC WAVE II equipment at room temperature, using aqueous suspensions of the obtained powders (the pH of those aqueous suspension was adjusted with 0.1 M NaOH). High-resolution transmission electron microscopy (HR-TEM) analysis of the materials was performed with a JEOL- 200 CX microscope operating at 80 KV. The aqueous suspensions of the materials after the purification steps were characterized by UV–vis spectrophotometry (Aquamate Thermo Spectronic spectrophotometer). The photoluminescence emission spectra of these aqueous suspensions were measured in a Horiba fluorimeter (FluoroMax-4) using 375 nm as excitation wavelength. Nuclear magnetic resonance (NMR) spectra of the 5:5kDa aqueous suspension were measured on a Bruker Avance III 500 MHz equipment for ^{1}H (500 MHz) and ^{13}C (125 MHz) nuclei in deuterium oxide (D_2O, 99.8 %).

3. Results and discussion

3.1. Choice of the membranes

Carbon dots were obtained upon microwave-assisted hydrothermal synthesis using orange peel waste. The aqueous solutions recovered after the hydrothermal treatment of the precursor were sequentially filtered in successive steps with membranes of cut-offs between 0.22 μm and 5

kDa (covering microfiltration and ultrafiltration membranes). It is important to point out that these membranes are a popular choice in the purification of carbon dots [3,27–31], despite they cover a fairly large range of dimensions, out of the nanometric dimensions of quantum dot materials (i.e., below 10 nm). Even if the correlation between a two-dimension particle size (nm) and a three-dimension molecular weight (kDa) is not straightforward, it is possible to estimate a relationship according to the literature (Fig. 1) [14,23,31,32]. A few examples are shown in Figure 1, and a more exhaustive list of studies correlating molecular cut-offs with the size of carbon dots is compiled in Table S1.

For instance, Essner *et al.* reported a correlation between the molecular weight and the size of colloidal fluorescent carbon dots, estimating that particles with 3–8 nm diameter size would correspond to a molecular weight between 15 and 40 kDa [14]. On the other hand, Hu *et al.* reported particles of 1.4±0.2 and 3.3±0.5 nm associated to molecular weights of 2.4 and 7.7 kDa, respectively [6]. Computational studies on carbon dots have also associated particle sizes between 0.5 and 5.5 nm with molecular weights between 0.1 and 10.8 kDa, corresponding to CxHy structures with x between 8–862 and y between 6–480 atoms [23]. Fig. 1 illustrates that the first two membranes used in this work (cut-off of 0.22 and 0.1 µm) allow to reject aggregates/particles in the suspensions between 220 and 100 nm size. Further sequential separation with ultrafiltration membranes of 100, 50 and 5 kDa cut-offs would allow to target carbon nanoparticles of sizes between 1.59 and 60 nm (Table S1).

Considering this, a theoretical average particle size of 10 nm would correspond to molecular weights below 100 kDa. Thus, the sequential separation carried out in this work with 100 kDa (step 3), 50 kDa (step 4) and 5 kDa (step 5) membranes is expected to ensure the rejection of the large carbonaceous particles typically formed during hydrothermal transformation of biomass, as well as many of the aromatic compounds that are formed during the decomposition of the biomass precursor (e.g., lignin, cellulose/hemicellulose derivatives, polysaccharides, polyphenols, carbohydrates) [33–39].

3.2. *Synthesis Yield*

Table 1 shows the yield of recovered solids in the synthesis and the ionic conductivity of the aqueous suspensions after the different filtration steps. The yield of the recovered solid fraction after the sequential filtration steps was quantified from absorbance measurements of resuspended aqueous dispersions after the freeze drying (the linear correlations are shown in Figure S1). Data of the synthesis without the acid

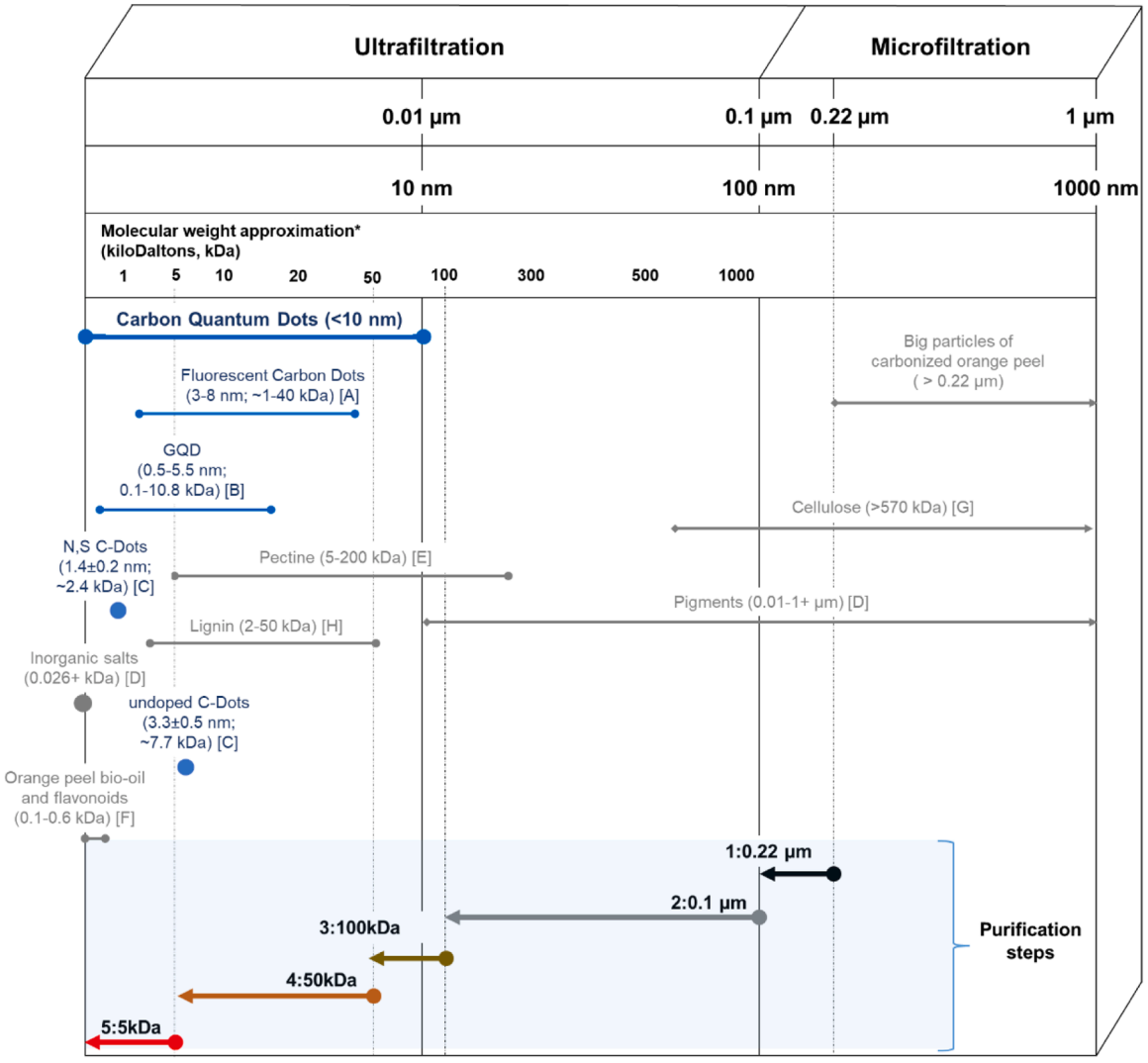

Fig. 1. Illustrative correlation between the molecular cut-off of different membranes used in the sequential filtration, and the average particle size of carbon dots. Molecular weights of relevant compounds formed in the degradation of biomass (i.e., the precursor used in this study for the synthesis of the carbon dots) are also included for comparison purposes.

Table 1
Yield of recovered solids, pH and ionic conductivity of the aqueous suspensions obtained from each sequential filtration step.

	Filtration step	Recovered solids [wt. %]	pH	Ionic conductivity [μS cm^{-1}]
without acid pre-treatment	1: 0.22 μm	16 ± 6	3.5	661
With acid pre-treatment	1: 0.22 μm	60 ± 36	3.3	301
	2: 0.1 μm	25 ± 8	3.4	301
	3: 100 kDa	16 ± 6	3.4	298
	4: 50 kDa	48 ± 12	3.5	276
	5: 5 kDa	36 ± 24	3.9	275

pre-treatment after filtration with a 0.22 μm membrane is also shown for comparison.

As described above, before the hydrothermal treatment, the precursor was initially treated in an acidic medium to decrease its large inorganic content (e.g., Ca, K, Mg, Na, P, S; Table S2). Otherwise, most of these inorganics are solubilized during the hydrothermal treatment and accumulate in solid fraction containing the carbon dots after the freeze-drying step, constituting a large fraction of inorganic impurities [2].

It is interesting to observe that the total solid yield obtained from the carbon precursor subjected to the acid treatment (60 ± 36 %) was larger than that of the untreated biomass (16 ± 6 %). This suggests that the lignocellulosic fraction of the orange peel was the main source of carbon for the synthesis of CDs, which is consistent with the amount of these components in the biomass before (~29.2 %) and after the acidic treatment (~79.7 %). Our previous studies have shown that acidic pH and oxidizing environments facilitate the formation of carbon dots from the microwave-assisted hydrothermal treatment of the lignocellulosic fraction of orange peels [2].

On the other hand, the yield of solids in suspension at each purification step did not change significantly with the number of membranes employed. It should be recalled in here that the synthetic route was the same in all the cases, and that the difference among the dispersions is the filtration with the membranes. Hence, the similarities in the solid yields in the dispersions regardless the membrane cut-off suggests that the synthesis method did not favor the formation of large carbonaceous particles or aggregates (ca. above 10 nm), that would be removed upon the first two steps of the sequential separation. The pH of the dispersions remained around 3.5 and the values of the ionic conductivity slightly decreased with the number of filtration steps, although differences are subtle.

3.3. Particle size

The average particle size of the synthesized carbon dots was determined in the suspensions after the sequential filtering by Dynamic Light Scattering (Fig. 2) and in the solids by high resolution TEM (Fig. 3). The hydrodynamic diameter of the carbon dots was evaluated from aqueous suspensions of the prepared materials with a solid loading of 0.25 mg mL^{-1} and pH adjusted to 6 (Fig. 2, Figure S4). The solid loading and the pH were selected after optimization experiments to obtain a suspension stable enough to execute particle size measurements for all the samples; otherwise, a poor reproducibility of the determinations was obtained. For example, in highly concentrated dispersions a tendency of aggregation of the particles into large clusters are typically observed due to the favored interactions among the particles [47,48]. Furthermore, the hydrodynamic diameter for the 5:5kDa sample was also evaluated in a more diluted suspension to increase the stability of the nanometric particles in suspension (ca. 0.05 mg mL^{-1}, see Figure S5), obtaining similar profiles.

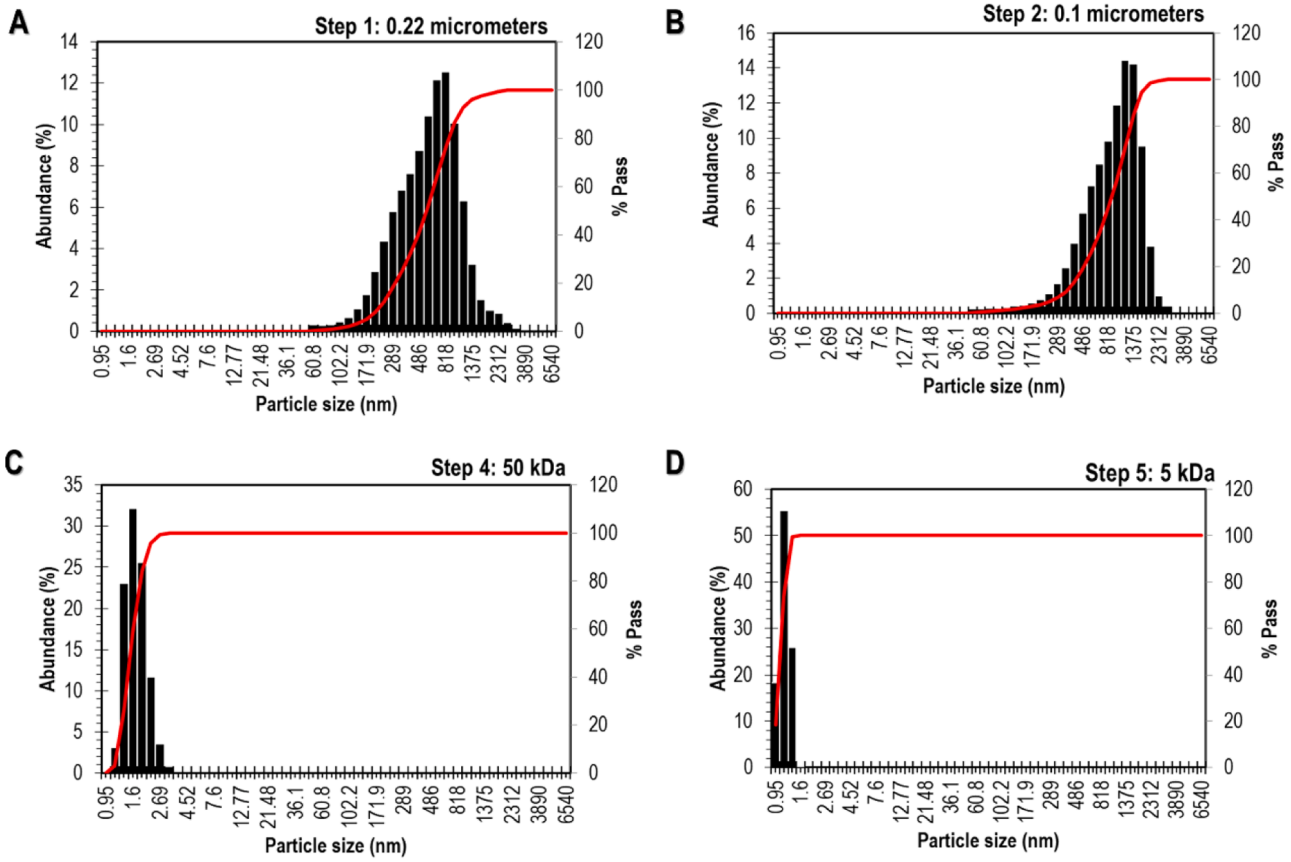

Fig. 2. Histograms of particle sizes obtained from Dynamic Light Scattering of the aqueous suspension of the solids recovered after the different filtration steps: (A) 0.22 μm; (B) 0.1 μm; (C) 50 kDa; (D) 5 kDa. Measurements correspond to 0.25 mg/mL aqueous suspensions (pH 6).

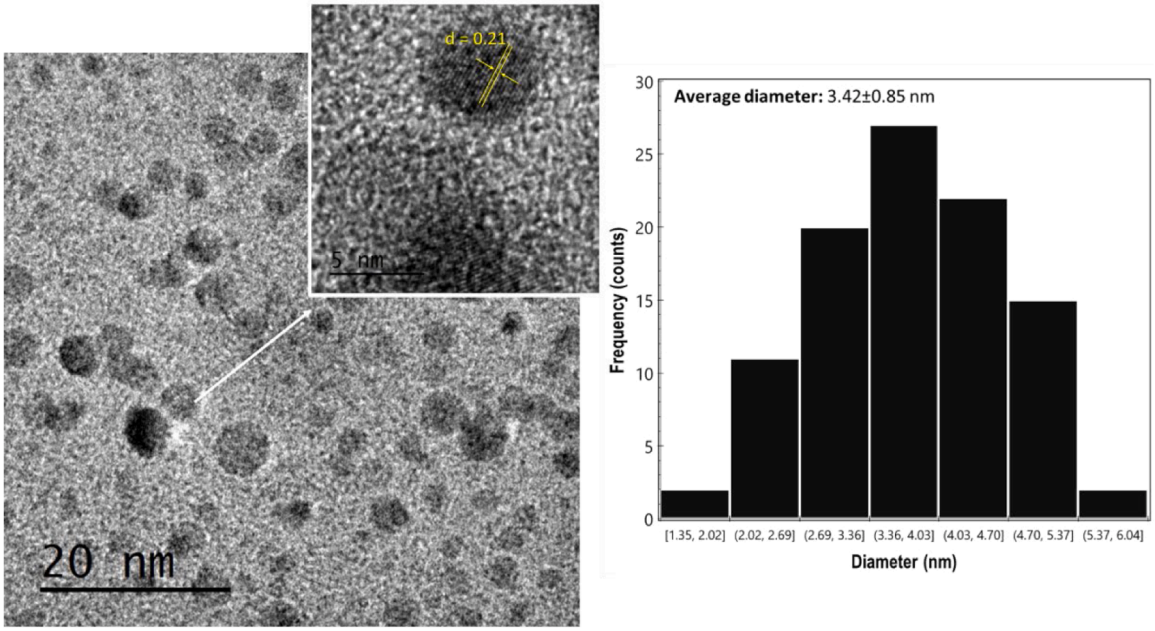

Fig. 3. High resolution TEM micrographs of the solid recovered after the sequential filtration step 5:5kDa at 0.05 mg/mL. Inset shows the interlayer distance of the carbon dots.

The first samples prepared upon one and two separation steps showed a wide distribution of particle sizes, compared to the rest of the series (ca. 500 nm for sample 1:0.22 μm and 800 nm for sample 2:0.1 μm). The range of particle sizes of these dispersions (Fig. 2A and B) was more than one order of magnitude higher than in the most purified samples (Fig. 2C and D, ca. below 10 nm in both cases). This points out the outstanding impact of the purification method in the eventual formation of large particle aggregates for a given composition. This is most likely due to the presence of oligomeric fragments in the suspension, that would favor interparticle interactions and/or interaction with the solvent of the suspension. Note that in this work only one experimental protocol has been used for the synthesis of carbon dots, and that the difference among the studied samples was the sequential separation with different membrane pore sizes and the number of separation steps on the same dispersion. These observations agree with reports in the literature on graphene oxide dots synthetized through microwave-assisted hydrothermal degradation of cellulose that showed properly dispersed nanometric suspensions at concentrations around 0.05 and 0.07 mg mL^{-1} [48]. It should be noted that carbon dots of smaller dimensions are typically produced when less complex precursors (e.g., organic commodities/monomers, citric acid, saccharides, etc.) and similar synthetic procedures are used [1,19]. This is due to the complexity of biomass, that involves the degradation of cellulose, condensation and polymerization of several aromatic molecules before the formation of stable carbon nanoparticles [27,28].

To corroborate the hydrodynamic particle diameter values obtained in the DLS studies, the sample obtained upon 5 separation steps (5:5 kDa) was further analyzed by high resolution transmission electron microscopy (Fig. 3). In agreement with the DLS results, a homogeneous dispersion of spherical nanoparticles with an average particle size of 3.42 ± 0.85 nm was observed (statistic measurement of at least 200 nanoparticles; Figure S5). In addition, the sample obtained from orange peel without washing after the first purification step was analyzed by Scanning Electron Spectroscopy revealing clusters larger than 500 nm (Figure S6). This observation is also consistent with the DLS measurements. The particles presented well-defined crystallographic planes with a d-spacing of 0.21 nm, that correspond to the (100) plane of graphitic carbon with sp^2 hybridization, as referenced in the crystallographic chart JCPDS 26-1076. Similar d-spacing values have been widely reported in the literature for CDs obtained from various biomass precursors [24,49–51].

3.4. Chemical characterization of the obtained fractions

After the filtration steps, the solid fraction was recovered by lyophilization, and it was further characterized. The FTIR spectra of the powders (Figure S2) revealed similar profiles in all the materials regardless the filtration step, with the characteristic bands corresponding to oxygen- and nitrogen-containing functional groups. This agrees with the elemental analysis of the precursor (Table S2). All the samples displayed a broad band centered at 3300 cm^{-1}, attributed to O-H stretching vibrations, along with two small bands centered at 2930 and 2880 cm^{-1}, attributed to stretching vibrations of sp^2 and sp^3 C-H. The band at 1725 cm^{-1} is associated with carboxylic acids, and the one around 1650 cm^{-1} could be related to stretching of N-H bonds, N-CO in amides and/or carbonyl groups from aldehydes or ketones. This is consistent with the presence of a small amount of nitrogen in the precursor (Table S2). The band around 1160 cm^{-1} -slightly more notorious for samples 3:100 kDa and 4:50 kDa- is assigned to the stretching of the C-O bonds. Besides, the band at 1020 cm^{-1} suggests the presence of primary alcohols; it could also be associated with the presence of sulfoxides (in agreement with the small amount of sulfur in the precursor, Table S2). The band centered around 1513 cm^{-1} is associated with aromatic carbon structures.

The thermal stability of the samples was rather similar regardless the filtration step, as inferred from the thermogravimetric profiles obtained under inert atmosphere (Fig. 4). The total mass loss after heating up to 1000 °C varied between 58 and 66 wt.%, following a subtle decreasing trend as the number of separation steps was increased (Table 2).

Various regions can be identified in the thermogravimetric profiles. The first region between 25 and 150 °C is attributed to the evolution of the moisture of the samples; the region between 150 and 600 °C corresponds to the decomposition of the carbonaceous matrix of the carbon dots. In general, the thermogravimetric profiles were rather similar for all the samples. In the range between 150 and 300 °C, a sharp peak was observed for all the samples, with mass losses increasing with the sequential filtration. This mass loss is typically associated to the evolution of the functional groups decorating the surface of the carbon dots

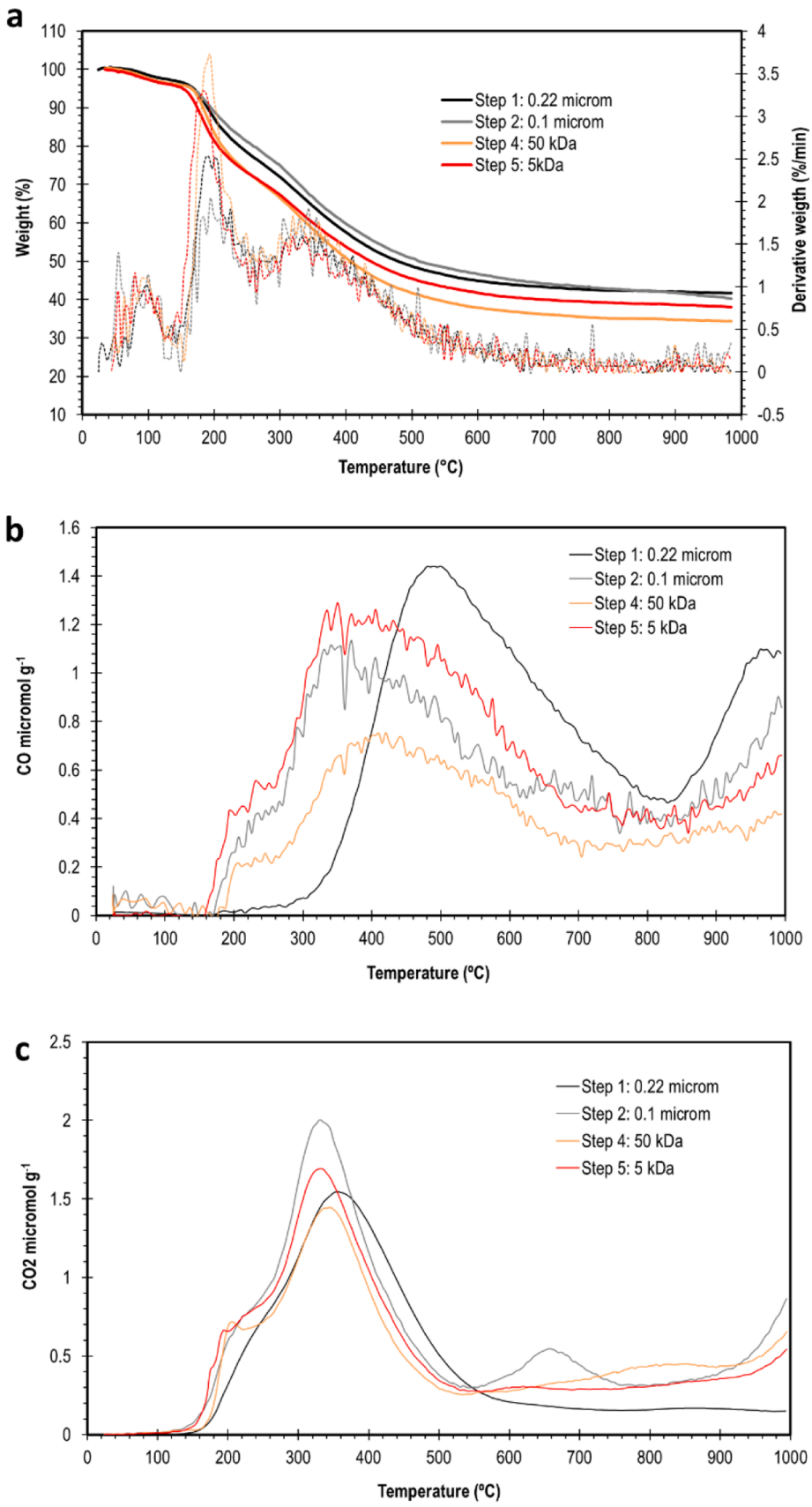

Fig. 4. Thermogravimetric profiles under inert atmosphere for the lyophilized solids recovered after each sequential purification steps; (b) CO (m/z28) and (c) CO_2 (m/z 44) evolution profiles detected in the mass spectrometer coupled to the thermobalance.

Table 2
Mass losses (wt.%) from the thermogravimetric profiles under inert atmosphere for different thermal ranges.

	Total Mass loss 25–1000°C [wt. %]	Mass loss 25–150 °C [wt. %]	Mass loss 150–300 °C [wt. %]	Mass loss 300–600 °C [wt. %]	Mass loss 600–1000 °C [wt. %]
Step 1: 0.22 μm	58.3	3.5	24.6	27.2	3.1
Step 2: 0.1 μm	59.8	4.2	25.8	27.7	6.2
Step 4: 50 kDa	65.7	4.2	34.2	28.0	3.4
Step 5: 5kDa	62.0	5.1	33.3	25.1	3.6

[40], as confirmed by the signals corresponding to m/z 28 and m/z 44 in the profiles (Fig. 4b,c). In the region between 300 and 600 °C, the mass losses ranged from 27 to 28 wt. %, with a slightly lower value for the most purified sample (5:5 kDa, ca. 25 wt. %). At temperatures above 600 °C the mass loss was low for all the samples (accounting for 3–6 wt. %).

The gases evolved from thermogravimetric analysis were characterized by mass spectrometry. The m/z ratio corresponding to CO and CO_2 are shown in Fig. 4, since these gases are related to the nature of the oxygen containing groups in carbon materials [40]. Other selected m/z in the range 50–300 are shown in Fig. 5 and Figure S3.

The profiles of CO and CO_2 evolution showed rather similar trends for all the samples, with some exceptions for the solids recovered after the first two microfiltration steps (1:0.22 μm and 2:0.1 μm). The profiles of the evolution of CO_2 showed a wide band between 200 and 550 °C for all the samples with small differences in the intensities, along with a shoulder at 150–200 °C. These bands are attributed to the decomposition of carboxylic acids of different acidic strength [41]. A small band above 600 °C was observed for sample 2:0.1 μm in the CO_2 profiles, which may be attributed to the decomposition of lactones [40]. The quantification of the amount of CO_2 evolved ranged from 400–550 micromol/g (Table 3), with slightly higher values for the samples with a higher number of purification steps.

The CO profiles showed a multimodal pattern with a first wide peak at temperatures between 200 and 600 °C, featuring a shoulder at 200–300 °C. A second peak was clearly observed above 800 °C for all the samples. The low temperature CO peaks are typically associated to the decomposition of carboxylic acids and anhydrides, while the evolution of CO at 400–700 °C is associated to phenolic groups, and that above 750 °C is associated with the presence of ether, carbonyl and quinone groups [40]. The shoulder around 150–250 °C in the CO profile may be ascribed to carboxylic acids, since it appears at the same temperatures in the CO_2 profiles; a similar assignment has been suggested in the literature for oxidized graphene flakes [41], although the origin of this peak is not fully understood. The low temperature peak in the CO profile (featuring around 200 °C) has also been assigned to the decomposition of hydroxyl groups in oxidized graphene-derivatives [41].

For selected samples (i.e., 1: 0.22 μm, 4: 50 kDa and 5: 5 kDa) the thermal decomposition profiles were recorded at m/z values ranging from 50 to 300. This range of m/z values would cover molecules typically found during the decomposition of biomass precursors [33–37], that could not be removed by the sequential separation with the membranes (Fig. 1). Selected m/z values are shown in Figure 5; the complete profiles of all detected m/z are shown in Figure S3.

It should be mentioned that in the range 50–300 m/z, only signals corresponding to selected m/z were detected: namely m/z 51–58, 65–68, 77–79, 81, 82, 91, 92, 95, 96, 105, 109, and 110 values. This indicates that subproducts with molecular weight higher than 110 and lower than 300 are not formed.

The m/z values of 53, 95 and 96 showed a bimodal shape, with a sharp peak between 150 and 200 °C and a broad band extending between 250 and 400 °C, in accordance with the thermogravimetric profiles. The intensity of the sharp peak observed at low temperature was more pronounced for the least filtrated samples. On the contrary, the intensity of the broad band was rather constant for all the samples. At m/z values of 54–57, only the band between 250 and 400 °C was observed with constant intensities in the samples, while at m/z of 58 the intensity of the band decreased with the purification step. These m/z values are associated with fragments of furfural, furanone and phenolic derivatives observed in the decomposition of biomass precursors [42], and could correspond to compounds like acetone, propenal or propenol. For the profiles corresponding to m/z values of 109 and 110, a sharp peak featuring between 150 and 250 °C, and to m/z values of 81 and 82, a broad peak between 250 and 450 °C were observed in all the samples. These fragments can be assigned to phenolic 1,2-bencenediol, anisole, cresols, and methyl-phenols derivatives, common subproducts detected in the degradation of biomass [43–46]. The intensity of the peak was rather similar for the samples after the first (0.22 μm) and fourth (50 kDa) separation steps, but was decreased substantially for the sample filtered at the fifth step (5 kDa), indicating the improving in the purification of the sequential separation with the 5 kDa membrane. These results also point out that the mass loss observed in the region 150–300 °C in the thermogravimetric profiles corresponds to the decomposition of the matrix of the carbon dots.

The most purified suspension (5:5kDa sample in aqueous suspension) was qualitatively analyzed by ^{1}H and ^{13}C Nuclear Magnetic Resonance (NMR) to determine the surface chemistry of the carbon dots. In this sense, the ^{1}H NMR spectrum (Figure S7) shows the presence of proton atoms attached to sp^3 hybridized carbon in the region from 0.5 to 6 ppm. The sp^3 carbon atoms were identified by their association with alkane protons and linked to ether, epoxy, carbonyl, amino, and amide functional groups. On the other hand, protons associated with carbon atoms with sp^2 hybridization were found in the region between 6 and 9 ppm and they were related to aromatic or aldehyde protons. Although this technique is not very sensitive, data suggests a higher ratio of sp^3 over sp^2 hybridization of carbon atoms.

This information was corroborated by ^{13}C NMR analysis. In the ^{13}C NMR spectrum a first zone between 10-105 ppm was also associated with sp^3 hybridized carbon atoms, corresponding to alkyl substituents (10 to 50 ppm), C-O and C-N single bonds in hydroxyl, amine, and amide groups (50–80 ppm) and carbons linked to ether, epoxide, and terminal C=C bonds (80–105 ppm). The region between 100–120 ppm is associated with sp^2 hybridized carbon atoms, and the signals between 150–190 ppm can be related to the presence of C=O bonds in amides, carboxylic acids, or aldehydes. In addition, a ^{13}C Attached Proton Test experiment (APT) was conducted with the aim to provide information regarding the number of hydrogen atoms bonded to a carbon atom. The APT spectra (Figure S7) revealed the signals attributed to the resonance of quaternary carbons and methylene groups (featuring as negative signals), while carbons bonded to an odd number of protons (e.g., methine, methyl groups) appear in the positive axis. Qualitative NMR analyzes corroborate in the carbon-based material the presence of sp^2 and sp^3 hybridized carbon atoms at the nanoscopic level corresponding to various functional groups, which has also been described with the thermal decomposition profiles and the FTIR spectroscopy.

3.5. *Optical properties of the suspensions*

The impact of the purification process on the optical properties of the carbon dots was assessed by UV–vis absorption spectrophotometry and photoluminescence emission spectroscopy (Fig. 6). Note that the UV–vis

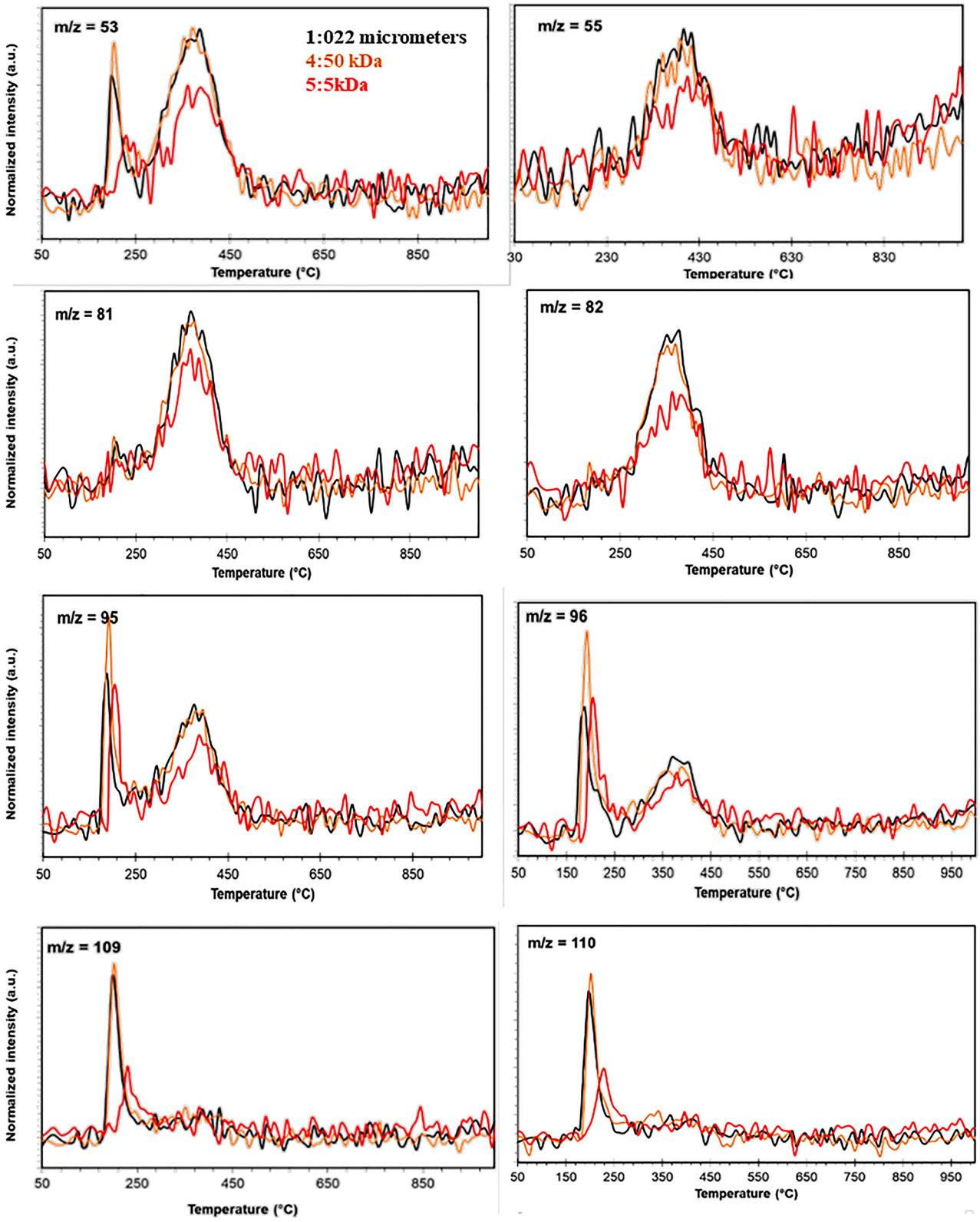

Fig. 5. Thermogravimetric profiles under inert atmosphere for the lyophilized solids recovered after each sequential purification steps corresponding to selected m/z signals.

absorption spectra give information about the amount of light absorbed, regardless is stabilization to the ground state through radiative or non-radiative transitions, whereas the photoluminescence spectroscopy provides information about the amount of light absorbed that follows a radiative transition (i.e., photoluminescence emission) to return to the fundamental state.

For comparison purposes, a solid loading of 0.25 mg mL^{-1} was selected for this study. This allows a proper comparison of the optical properties of the samples avoiding differences due to light re-absorption processes eventually occurring in concentrated suspensions. Fig. 6a

Table 3
Total amounts of CO_2 and CO released from the samples and determined by TPD –MS and total amount of oxygen obtained from TPD data (assuming that all the surface oxygen was released as CO and/or CO_2).

	CO (μmol g^{-1})	CO_2 (μmol g^{-1})	Oxygen (%)
1: 0.22 μm	587	410	32.6
2: 0.1 μm	522	559	33.5
4: 50 kDa	352	463	33.8
5: 5 kDa	580	481	33.0

shows the UV–vis absorption spectra of aqueous suspensions recovered at the different filtration steps. All the suspensions presented rather similar profiles, characterized by a broad absorption band in the UV region and a long tail extending to the visible region. The absorption band is characterized by a main peak located at 280 nm, and shoulders or less intense peaks at 220 and 340 nm. The peaks at 280 and 220 nm can be attributed to π-π* transitions of sp^2 carbon atoms (i.e., a graphitic carbon core), and the bands between 300–400 nm are attributed to n-π* transitions in C=O bonds (i.e., functionalized carbon atoms) [52].

The samples presented differences in the intensity of the absorbance even when all the dispersions were prepared with the same concentration. The absorbance of sample 2:0.1 μm was the highest among the series, suggesting the presence of a larger number of absorbing groups in the suspension. The intensity of the bands was somewhat decreasing with the number of separation steps, although differences are subtle. This suggests that only a small fraction of light absorbing species were removed during the purification steps, pointing out that the CDs matrix and the small molecules (<5 kDa) are the main responsible for the observed optical features (with a less contribution from the impurities removed during the microfiltration). Similar observations have been reported by Essner et al. on the purification of carbon dots derived from citric acid following a nanofiltration membrane processs. Essner *et al.* identified two different populations of fluorophores: the first one with sizes smaller than 1 kDa responsible of most of the fluorescence of the samples, and the second one of size smaller than 50 kDa, which were low quantum yield emitters [14].

The impact of the different purification steps was more clearly seen in the photoluminescence emission features of the samples. Fig. 6b shows the photoluminescence emission upon excitation at 375 nm of aqueous suspensions with 0.25 mg mL^{-1} after each separation step. The full dataset at different dilutions is shown in Figure S8.

The shape of the photoluminescence spectra was characterized by a broad emission with a maximum at ca. 450 nm and a pronounced shoulder at around 550 nm. The multimodal character of the emission spectra indicates the contribution of several fluorophores to the emission of the samples. The intensity of the emission at the maximum position (ca. 450 nm) did not show a clear correlation with the different filtration steps (trend: 2:0.1 μm >> 3:100 kDa >> 4:50 kDa ~ 1:0.22 μm > 5:5 kDa). The highest emission intensities were obtained for the sample after 2 steps of purification (membrane 0.1 μm), and the lowest one was measured for the most purified sample (membrane 5 kDa). This is important since it confirms that the photoluminescence emission of suspensions of carbon dots can be altered by the emission of other fluorophores present in the medium if the samples are not sufficiently purified. The emitting fluorophores removed during the sequential filtration may be related to presence of the compounds with m/z 53, 81–82, 96–96, 109–110 observed in the thermal fingerprint of the least purified samples (Fig. 5), and whose intensity decreased with the number of filtration steps.

Despite samples 1:0.22 μm and 3:100 kDa displayed rather similar absorbance features (Fig. 6a), the emission of sample 3:100 kDa was more pronounced than that of sample 1:0.22 μm. These differences may be related to quenching effects promoted by light-absorbing compounds involving non-radiative transitions in the least purified sample (1:0.22 μm).

Regardless the decrease in the intensity of the emission, the suspension of carbon dots in the most purified protocol still displayed a notorious emission upon excitation at 375 nm. The absolute quantum yields of the dispersions with 0.25 mg mL^{-1} upon excitation at 375 nm ranged between 3.4 % for the least purified sample and 5.2 % for the most purified one. These values, although are not among the highest reported for carbon dots, are comparable to those reported for non-metal doped carbon dots [53–55].

4. Conclusions

Carbon dots with average particle sizes of 3.5 nm and composed of a graphitic-like core decorated with oxygen and nitrogen moieties have been synthesized by a microwave-assisted hydrothermal treatment of orange peels. The application of a sequential filtration to the suspensions of those carbon dots with membranes of decreasing molecular cut-off has revelated the importance of the correct purification methods on the chemical composition and the photoluminescence emission features of the obtained carbon dots. A complete thermal characterization by TPD-MS of the solids recovered after each filtration step has demonstrated the presence of fragments assigned to different molecules (e.g., furfural and phenolic derivatives) released in the medium during the hydrothermal transformation of the precursor. The analysis of the average particle size by dynamic light scattering has highlighted the impact of the purification in the formation of large particle aggregates, responsible for a decrease in the intensity of the photoluminescence emission owing to self-absorbing and quenching effects. The aqueous suspension of the carbon dots recovered after the most purified protocol

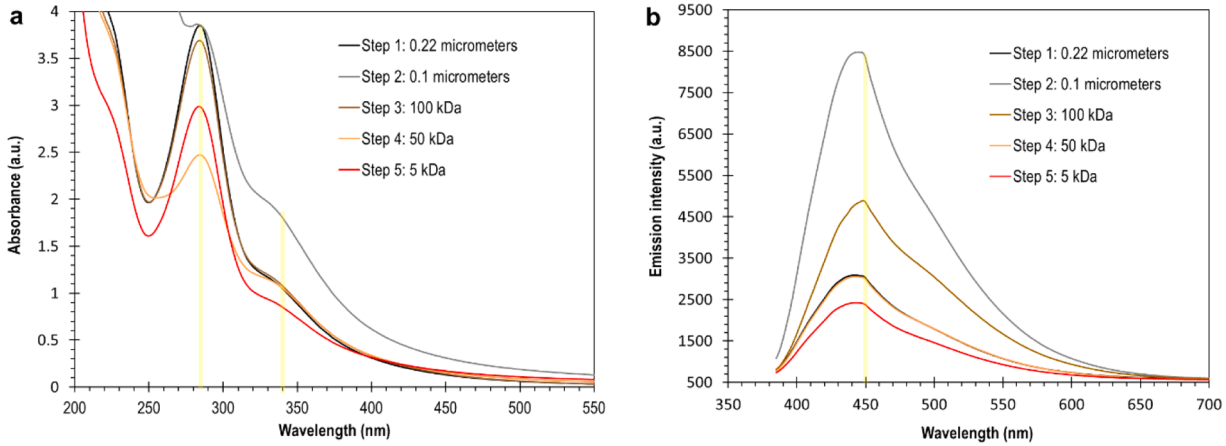

Fig. 6. (a) UV–vis and (b) photoluminescence spectra upon excitation at 375 nm of aqueous suspensions at 0.25 mg mL^{-1} after each separation step.

displayed a notorious emission upon excitation at 375 nm, confirming that the carbon dots were responsible for the observed optical features. All this highlights the importance of an adequate purification process to isolate carbon dots obtained from complex precursors (such as biomass), to avoid bias interpretation of the photoluminescence properties of these materials.

Data and code availability

Not Applicable

Ethical approval

Not Applicable

Supporting Information Description

Table S1. Literature survey of scientific articles reporting the use of membranes with molecular cut-off lower than 5 kDa that obtain carbon dots with particle sizes between 1.5–60 nm. Table S2. Composition of the orange peel used as precursor for the synthesis of carbon dots, before and after the acid wash. Figure S1. Absorbance values of aqueous suspensions of the solid fractions recovered at the different filtration steps. Dilutions were made for the quantification of the synthesis yields. Figure S2. FTIR-ATR spectra of the lyophilized powders obtained after the sequential separation steps. Figure S3. Thermogravimetric profiles corresponding to selected m/z signals for the solids recovered after different steps of filtration. Figure S4. Histograms of particle sizes obtained from Dynamic Light Scattering of aqueous suspension of the solids recovered after the sequential filtration step 5:5 kDa. Measurements correspond to 0.05 mg/mL aqueous suspensions (pH 6). Figure S5. Counting of 200 nanoparticles from high resolution TEM on the solid recovered after the sequential filtration step 5:5kDa at 0.05 mg/mL. Figure S6. Scanning Electron Microscopy micrographs of the solid recovered after the sequential filtration 1: 0.22 micrometers. Figure S7. ^{1}H NMR spectrum of carbon dots from separation step 5:5 kDa in D_2O at 500 MHz (A) and with water suppression (B) in D_2O at 500 MHz. $^{13}C\{^{1}H\}$-NMR spectrum of carbon dots obtained from separation step 5:5 kDa (C) and $^{13}C\{^{1}H\}$-APT NMR spectrum (D) in D_2O at 125 MHz. Figure S8. Photoluminescence emission spectra of aqueous suspensions of the solids recovered after sequential filtration steps, upon excitation at 375 nm.

CRediT authorship contribution statement

Andrea S. Gonzalez-Vera: Writing – review & editing, Writing – original draft, Methodology, Formal analysis, Conceptualization. **Carlos A. Pineda-Arellano:** Writing – review & editing. **Armando Ramírez-Monroy:** Writing – review & editing. **J. Matos:** Writing – review & editing. **Luis F. Chazaro-Ruiz:** Writing – review & editing, Supervision, Resources, Methodology, Conceptualization. **J. Rene Rangel-Mendez:** Writing – review & editing, Supervision, Resources, Methodology, Conceptualization. **Conchi O. Ania:** Writing – review & editing, Writing – original draft, Resources, Funding acquisition, Formal analysis, Conceptualization.

Declaration of competing interest

The authors declare that they have no known competing financial interests or personal relationships that could have appeared to influence the work reported in this paper.

Acknowledgments

The authors thank the financial support of CONACYT-Fondos Sectoriales-SENER (grant 245467), SEP CONACYT ANUIES and ECOS NORD (grants 315202, M20P01), ANID-ANILLO (grant ATE220014) and the Romanian Ministry of Research, Innovation and Digitization (PNRR-III-C9-2022-I8-291, grant 760081/23.05.2023). Gonzalez-Vera thanks CONAHCYT for her PhD scholarship (CVU 821870). The authors also thank LAMBAMA, LINAN and IPICYT laboratories for the facilities and the technical support (M. Rocha-Medina, E. Isaacs-Paez, G. Vidriales-Escobar, H. Silva-Pereyra, M. Olvera-Sosa).

Supplementary materials

Supplementary material associated with this article can be found, in the online version, at doi:10.1016/j.cartre.2025.100460.

References

[1] W. Xu, F. Zeng, Q. Han, Peng, Recent advancements of solid-state emissive carbon dots: A review, Coord. Chem. Rev. 498 (2024) 215469, https://doi.org/10.1016/j.ccr.2023.215469.
[2] P.M. Olmos-Moya, S. Velazquez-Martinez, C. Pineda-Arellano, J.R. Rangel-Mendez, L.F. Chazaro-Ruiz, High added value functionalized carbon quantum dots synthetized from orange peels by assisted microwave solvothermal method and their performance as photosensitizer of mesoporous TiO_2 photoelectrodes, Carbon 187 (2022) 216–229, https://doi.org/10.1016/j.carbon.2021.11.003.
[3] T. Chatzimitakos, A. Kasouni, L. Sygellou, A. Avgeropoulos, A. Troganis, C. Stalikas, Two of a kind but different: Luminescent carbon quantum dots from Citrus peels for iron and tartrazine sensing and cell imaging, Talanta 175 (2017), https://doi.org/10.1016/j.talanta.2017.07.053.
[4] M. Wang, R. Shi, M. Gao, K. Zhang, L. Deng, Q. Fu, L. Wang, D. Gao, Sensitivity fluorescent switching sensor for Cr (VI) and ascorbic acid detection based on orange peels-derived carbon dots modified with EDTA, Food Chem. 318 (2020), https://doi.org/10.1016/j.foodchem.2020.126506.
[5] F.M. Abdoon, H.M. Atawy, Prospective of microwave-assisted and hydrothermal synthesis of carbon quantum dots/silver nanoparticles for spectrophotometric determination of losartan potassium in pure form and pharmaceutical formulations, in: Mater Today Proc, Elsevier Ltd, 2021, pp. 2141–2149, https://doi.org/10.1016/j.matpr.2020.12.298.
[6] X. Hu, Y. Li, Y. Xu, Z. Gan, X. Zou, J. Shi, X. Huang, Z. Li, Y. Li, Green one-step synthesis of carbon quantum dots from orange peel for fluorescent detection of Escherichia coli in milk, Food Chem. 339 (2021), https://doi.org/10.1016/j.foodchem.2020.127775.
[7] B. Acharya, A. Behera, S. Behera, S. Moharana, Carbon quantum dots: A systematic overview of recent developments in synthesis, properties, and novel therapeutic applications, Inorg. Chem. Commun. 165 (2024), https://doi.org/10.1016/j.inoche.2024.112492.
[8] Y. Liu, H. Huang, W. Cao, B. Mao, Y. Liu, Z. Kang, Advances in carbon dots: From the perspective of traditional quantum dots, Mater. Chem. Front. 4 (2020) 1586–1613, https://doi.org/10.1039/d0qm00090f.
[9] Á.J. García-Salcedo, L.A. Giraldo-Pinto, D.J. Márquez-Castro, L. Tirado-Mejía, Influence of synthesis parameters on the optical properties of carbon dots, Carbon Trends 17 (2024) 100403, https://doi.org/10.1016/j.cartre.2024.100403.
[10] M. Motamedi, X. Zheng, P. Koshy, R.A. Taylor, Synthesis and thermophysical property characterization of aqueous graphene quantum dot dispersions for air-conditioning applications, Carbon Trends 16 (2024) 100372, https://doi.org/10.1016/j.cartre.2024.100372.
[11] K. Zuo, W. Liu, X. Liu, X. Liu, Phosphorescence of carbon dot: the intrinsic mechanism and recent progress, Carbon Trends 12 (2023) 100278, https://doi.org/10.1016/j.cartre.2023.100278.
[12] M. Kurian, A. Paul, Recent trends in the use of green sources for carbon dot synthesis–A short review, Carbon Trends 3 (2021) 100032, https://doi.org/10.1016/j.cartre.2021.100032.
[13] S. Jing, Y. Zhao, R.C. Sun, L. Zhong, X. Peng, Facile and high-yield synthesis of carbon quantum dots from biomass-derived carbons at mild condition, ACS. Sustain. Chem. Eng. 7 (2019) 7833–7843, https://doi.org/10.1021/acssuschemeng.9b00027.
[14] J.B. Essner, J.A. Kist, L. Polo-Parada, G.A. Baker, Artifacts and errors associated with the ubiquitous presence of fluorescent impurities in carbon nanodots, Chem. Materials 30 (2018) 1878–1887, https://doi.org/10.1021/acs.chemmater.7b04446.
[15] J. Zhu, C. Wu, Y. Cui, D. Li, Y. Zhang, J. Xu, C. Li, S. Iqbal, M. Cao, Blue-emitting carbon quantum dots: Ultrafast microwave synthesis, purification and strong fluorescence in organic solvents, Colloids. Surf. a Physicochem. Eng. Asp. 623 (2021), https://doi.org/10.1016/j.colsurfa.2021.126673.
[16] A. Beiraghi, S.A. Najibi-Gehraz, Purification and fractionation of carbon dots using ph-controlled cloud point extraction technique, J. Nanostruct. 10 (2020) 107–118, https://doi.org/10.22052/JNS.2020.01.012.
[17] K. Mishra, M. Barai, S. Ghosh, Roles of impurity and sample heterogeneity in intriguing photoluminescence properties of zero-dimensional (0D) Carbonaceous Materials, J. Phys. Chem. C (2022), https://doi.org/10.1021/acs.jpcc.2c05477.
[18] B. Thangaraj, P.R. Solomon, S. Chuangchote, N. Wongyao, W. Surareungchai, Biomass-derived carbon quantum dots – a review. part 1: preparation and characterization, ChemBioEng Rev. 8 (2021) 265–301, https://doi.org/10.1002/cben.202000029.
[19] C. Ji, Q. Han, Y. Zhou, J. Wu, W. Shi, L. Gao, R.M. Leblanc, Z. Peng, Phenylenediamine-derived near infrared carbon dots: The kilogram-scale

preparation, formation process, photoluminescence tuning mechanism and application as red phosphors, Carbon 192 (2022) 198–208, https://doi.org/10.1016/j.carbon.2022.02.054.
[20] J.C. Crittenden, R.R. Trussell, D.W. Hand, K.J. Howe, G. Tchobanoglous, MWH's Water treatment: Principles and Design, John Wiley & Sons, 2012.
[21] M. Cheryan, Ultrafiltration and Microfiltration Handbook, Technomic, Lancaster, PA, n.d.
[22] X. Wang, X. Zhang, G. Zhou, J. Qian, Z. Li, W. Li, Feasibility study on the separation and purification of sinomenine hydrochloride from Caulis sinomenii solution based on membrane ultrafiltration technology, Sustain. Chem. Pharm. 39 (2024) 101549, https://doi.org/10.1016/j.scp.2024.101549.
[23] M.A. Sk, A. Ananthanarayanan, L. Huang, K.H. Lim, P. Chen, Revealing the tunable photoluminescence properties of graphene quantum dots, J. Mater. Chem. C. Mater. 2 (2014) 6954–6960, https://doi.org/10.1039/c4tc01191k.
[24] K.K. Gudimella, T. Appidi, H.F. Wu, V. Battula, A. Jogdand, A.K. Rengan, G. Gedda, Sand bath assisted green synthesis of carbon dots from citrus fruit peels for free radical scavenging and cell imaging, Colloids. Surf. B Biointerfaces. 197 (2021), https://doi.org/10.1016/j.colsurfb.2020.111362.
[25] A. Prasannan, T. Imae, One-pot synthesis of fluorescent carbon dots from orange waste peels, Ind. Eng. Chem. Res. (2013) 15673–15678, https://doi.org/10.1021/ie402421s.
[26] A.N.L. Tiong, N.K.H. Wong, J.F.Y. Fong, X.W. Tan, S.M. Ng, A sustainable alternative to synthesis optical sensing receptor for the detection of metal ions, Opt. Mater. (Amst) 40 (2015) 132–138, https://doi.org/10.1016/j.optmat.2014.12.021.
[27] G. Yang, X. Wan, Y. Su, X. Zeng, J. Tang, Acidophilic S-doped carbon quantum dots derived from cellulose fibers and their fluorescence sensing performance for metal ions in an extremely strong acid environment, J. Mater. Chem. a Mater. 4 (2016) 12841–12849, https://doi.org/10.1039/c6ta05943k.
[28] S.K. Das, S. Chakrabarty, R. Gawas, K. Jasuja, Serendipitous formation of photoluminescent carbon quantum dots by mere immersion of a polymer in an organic solvent, Carbon Trends 8 (2022), https://doi.org/10.1016/j.cartre.2022.100183.
[29] S. Ganesan, R. Kalimuthu, T. Kanagaraj, R. Kulandaivelu, R. Nagappan, L. A. Pragasan, V.K. Ponnusamy, Microwave-assisted green synthesis of multi-functional carbon quantum dots as efficient fluorescence sensor for ultra-trace level monitoring of ammonia in environmental water, Environ. Res. 206 (2022), https://doi.org/10.1016/j.envres.2021.112589.
[30] M.S. Devi, T.D. Thangadurai, N. Manjubaashini, D. Nataraj, Walnut shell biomass waste derived excitation-dependent CDs for toxic insecticide sensing and protein denaturation inhibition – An ecofriendly and sustainable approach, Diam. Relat. Mater. 136 (2023), https://doi.org/10.1016/j.diamond.2023.110021.
[31] Q. Hu, M.C. Paau, Y. Zhang, X. Gong, L. Zhang, D. Lu, Y. Liu, Q. Liu, J. Yao, M.M. F. Choi, Green synthesis of fluorescent nitrogen/sulfur-doped carbon dots and investigation of their properties by HPLC coupled with mass spectrometry, RSC. Adv. 4 (2014) 18065–18073, https://doi.org/10.1039/c4ra02170c.
[32] Spectrum Labs, Laboratory Product Catalog, (2012). https://www.laboplus.pl/wp-content/uploads/2019/12/2012-Katalog-Spectrum.pdf (accessed January 29, 2024).
[33] M. Zioga, E. Tsouko, S. Maina, A. Koutinas, I. Mandala, V. Evageliou, Physicochemical and rheological characteristics of pectin extracted from renewable orange peel employing conventional and green technologies, Food Hydrocoll. 132 (2022), https://doi.org/10.1016/j.foodhyd.2022.107887.
[34] S.E. Harding, G. Berth, A. Ball, J.R. Mitchell, J.G. de la Torre, The molecular weight distribution and conformation of citrus pectins in solution studied by hydrodynamics, Carbohydr. Polym. 16 (1991) 1–15, https://doi.org/10.1016/0144-8617(91)90069-O.
[35] R. Miranda, D. Bustos-Martinez, C.S. Blanco, M.H.G. Villarreal, M.E.R. Cantú, Pyrolysis of sweet orange (Citrus sinensis) dry peel, J. Anal. Appl. Pyrolysis. 86 (2009) 245–251, https://doi.org/10.1016/j.jaap.2009.06.001.
[36] S.M.S. Sawalha, D. Arráez-Román, A. Segura-Carretero, A. Fernández-Gutiérrez, Quantification of main phenolic compounds in sweet and bitter orange peel using CE-MS/MS, Food Chem. 116 (2009) 567–574, https://doi.org/10.1016/j.foodchem.2009.03.003.
[37] J. Xie, Q. Cao, W. jun Wang, H. yan Zhang, B. Deng, Understanding changes in volatile compounds and fatty acids of Jincheng orange peel oil at different growth stages using GC–MS, J. Integr. Agric. 22 (2023) 2282–2294, https://doi.org/10.1016/j.jia.2023.05.015.
[38] E.O. Kraemer, Molecular weights of celluloses and cellulose derivates, Ind. Eng. Chem. 30 (1938) 1200–1203, https://doi.org/10.1021/ie50346a023.
[39] A. Wypych, in Lignin, Databook of Adhesion Promoters, Elsevier, 2023, p. 149, https://doi.org/10.1016/B978-1-77467-012-5.50019-6.
[40] R.P. Rocha, M.F.R. Pereira, J.L. Figueiredo, Characterisation of the surface chemistry of carbon materials by temperature-programmed desorption: An assessment, Catal. Today 418 (2023), https://doi.org/10.1016/j.cattod.2023.114136.
[41] M.P. Araújo, O.S.G.P. Soares, A.J.S. Fernandes, M.F.R. Pereira, C. Freire, Tuning the surface chemistry of graphene flakes: new strategies for selective oxidation, RSC. Adv. 7 (2017) 14290–14301, https://doi.org/10.1039/c6ra28868e.
[42] Y.Le Brech, L. Jia, S. Cissé, G. Mauviel, N. Brosse, A. Dufour, Mechanisms of biomass pyrolysis studied by combining a fixed bed reactor with advanced gas analysis, J. Anal. Appl. Pyrolysis. 117 (2016) 334–346, https://doi.org/10.1016/j.jaap.2015.10.013.
[43] C. Castilla, C.P. Rüger, H. Lavanant, C. Afonso, Ion mobility mass spectrometry of in situ generated biomass pyrolysis products, J. Anal. Appl. Pyrolysis. 156 (2021), https://doi.org/10.1016/j.jaap.2021.105164.
[44] E. Christensen, R.J. Evans, D. Carpenter, High-resolution mass spectrometric analysis of biomass pyrolysis vapors, J. Anal. Appl. Pyrolysis. 124 (2017) 327–334, https://doi.org/10.1016/j.jaap.2017.01.015.
[45] M.A. Fahmey, M.A. Zayed, Y.H. Keshk, Comparative study on the fragmentation of some simple phenolic compounds using mass spectrometry and thermal analyses, 2001.
[46] P. Li, S. Xue, L. Sun, X. Zong, L. An, D. Qu, X. Wang, Z. Sun, Formation and fluorescent mechanism of red emissive carbon dots from o-phenylenediamine and catechol system, Light. Sci. Appl. 11 (2022), https://doi.org/10.1038/s41377-022-00984-5.
[47] J. Lim, S.P. Yeap, H.X. Che, S.C. Low, Characterization of magnetic nanoparticle by dynamic light scattering, Nanoscale Res. Lett. 8 (2013), https://doi.org/10.1186/1556-276X-8-381.
[48] S. Hassanzadeh, K.H. Adolfsson, M. Hakkarainen, Controlling the cooperative self-assembly of graphene oxide quantum dots in aqueous solutions, RSC. Adv. 5 (2015) 57425–57432, https://doi.org/10.1039/c5ra09704e.
[49] W. Lu, X. Qin, S. Liu, G. Chang, Y. Zhang, Y. Luo, A.M. Asiri, A.O. Al-Youbi, X. Sun, Economical, green synthesis of fluorescent carbon nanoparticles and their use as probes for sensitive and selective detection of mercury(II) ions, Anal. Chem. 84 (2012), https://doi.org/10.1021/ac3007939.
[50] J. Xu, P. Zhou, L. Yuan, X. Liu, J. Ma, C. Zhang, Dual lignin valorization enabled by carbon quantum dots and lithium-sulfur cathode, Ind. Crops. Prod. 170 (2021), https://doi.org/10.1016/j.indcrop.2021.113801.
[51] P. Wu, W. Li, Q. Wu, Y. Liu, S. Liu, Hydrothermal synthesis of nitrogen-doped carbon quantum dots from microcrystalline cellulose for the detection of Fe3+ ions in an acidic environment, RSC. Adv. 7 (2017) 44144–44153, https://doi.org/10.1039/c7ra08400e.
[52] W. Liu, C. Li, X. Sun, W. Pan, G. Yu, J. Wang, Highly crystalline carbon dots from fresh tomato: UV emission and quantum confinement, Nanotechnology. 28 (2017), https://doi.org/10.1088/1361-6528/aa900b.
[53] L. Zhang, X. Yang, Z. Yin, L. Sun, A review on carbon quantum dots: Synthesis, photoluminescence mechanisms and applications, Luminescence 37 (2022) 1612–1638, https://doi.org/10.1002/bio.4351.
[54] C. Stan, N. Elouakassi, C. Albu, C. Ania, A. Coroaba, L. Ursu, M. Popa, H. Kaddami, A. Almaggoussi, Photoluminescence of argan-waste-derived carbon nanodots embedded in polymer matrices, Nanomaterials 14 (2023) 83, https://doi.org/10.3390/nano14010083.
[55] K.G. Nguyen, I.A. Baragau, R. Gromicova, A. Nicolaev, S.A.J. Thomson, A. Rennie, N.P. Power, M.T. Sajjad, S. Kellici, Investigating the effect of N-doping on carbon quantum dots structure, optical properties and metal ion screening, Sci. Rep. 12 (2022), https://doi.org/10.1038/s41598-022-16893-x.